Proceedings of ASME Turbo Expo 2000:
International Gas Turbine & Aeroengine Congress & Exhibition
May 8-11, 2000, Munich, Germany

2000-GT-0374

PREDICTION OF LOW ENGINE ORDER INLET DISTORTION DRIVEN RESONANCE IN A LOW ASPECT RATIO FAN

J.G. Marshall
Rolls-Royce plc, Derby, UK

L. Xu
Whittle Laboratory, Cambridge University, UK

J. Denton
Whittle Laboratory, Cambridge University, UK

J.W. Chew
Rolls-Royce plc, Derby, UK

ABSTRACT

This paper presents a forced response prediction of 3 resonances in a low aspect ratio modern fan rotor and compares with other worker's experimental data. The incoming disturbances are due to low engine-order inlet distortion from upstream screens. The resonances occur in the running range at 3 and 8 engine orders which cross low modes (flap, torsion and stripe) of the blade. The fan was tested with on-blade instrumentation at both on- and off-resonant conditions to establish the unsteady pressures due to known distortion patterns.

The resulting steady and unsteady flow in the fan blade passages has been predicted by three methods, all three-dimensional. The first is a linearised unsteady Euler method; the second is a non-linear unsteady Navier-Stokes method; the third method uses a similar level of aerodynamic modelling as the second but also includes a coupled model of the structural dynamics. The predictions for the 3 methods are presented against the test data, and further insight into the problem is obtained through post-processing of the data. Predictions of the blade vibration response are also obtained. Overall the level of agreement between calculations and measurements is considered encouraging although further research is needed.

INTRODUCTION

Forced response in turbomachinery blading is a complex phenomenon. It is usually clear from the Campbell diagram where resonances are likely to occur, but it is not necessarily clear which resonant crossings are likely to produce unacceptable vibrations that will compromise the life of the component. This is due to the fact that the amplitude of the forcing at different engine orders is difficult to predict, even for cases where it is clear what is causing the particular forcing (e.g. vane number), and particularly where it is not (e.g. low engine order forcing). Moreover, the aerodynamic forcing may be affected by the blade vibration itself (through aerodynamic damping), and the blade motion may be complicated by non-linear friction damping in the roots and shrouds (some of which may be deliberately introduced to limit the vibration). Another complication is the effect of small differences in manufacture of individual blades. This leads to the so-called mistuning of the assembly (both mechanical and aerodynamic) which may mean that the vibration amplitude of the 'worst' blade may be several times that of the 'best'. Thus the lifing criterion must be based on the worst case rather than the mean or 'tuned assembly' values.

In this paper, state-of-the-art prediction methods are compared with experimental data for the first rotor in a 2-stage fan. In fans it is not usually possible to arrange for all resonances to be out of the running range owing to the wide range of speeds and operating conditions required. Forced response may arise due to both excitations from variable vanes and due to inlet or exit distortions. Potential costs of redesigning to correct these problems are large, and so it is important that predictive techniques are developed so that potential problems can be identified and addressed in the design stage.

The particular fan considered is the Augmented Damping Low Aspect Ratio Fan (ADLARF) tested at the Wright-Patterson Air Force Base and described in several earlier publications. See, for example, Woehr and Manwaring (1994), Rabe et al (1995) and Manwaring et al (1996). This fan has been used for a variety of research in the United States, and the geometry has recently been made available to the present authors through collaboration with the US Air Force and the UK Ministry of Defence. A schematic of the test configuration is reproduced in fig. 1. Attention here is confined to the effects of inlet distortion on the undamped fan. The distortion is

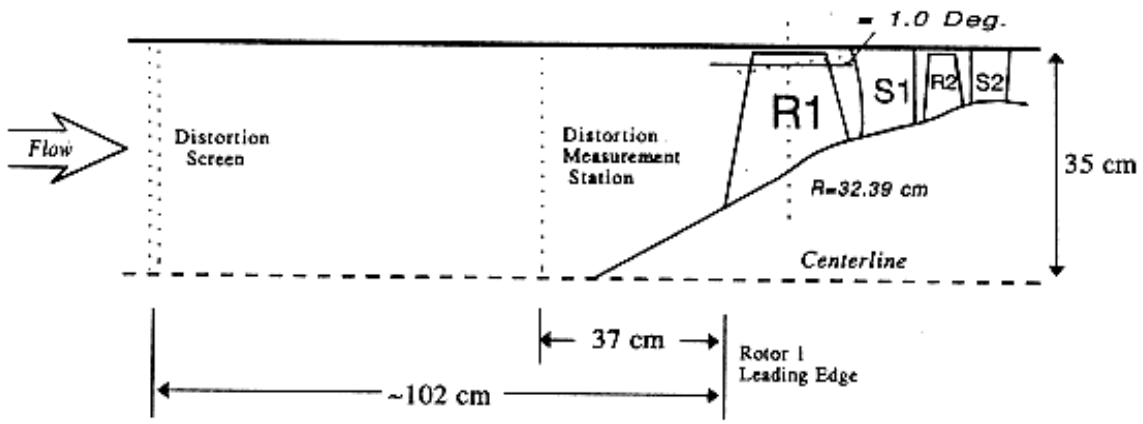

Fig. 1. Schematic of ADLARF test configuration

created by upstream screens giving circumferential distortions of 3 and 8 periods per revolution. The first rotor has 16 blades and the stage pressure ratio is around 2.4. Measurements available include unsteady blade pressures and strain gauges.

The papers by Manwaring et al (1996) and Hah et al (1996) are particularly relevant to the present contribution. Both these references present experimental data and include comparisons with computational fluid dynamics (CFD) predictions for the first rotor of the ADLARF fan. Manwaring et al used a 3D CFD model to calculate steady flow, and then applied a quasi-3D linearised, unsteady Euler solver to calculate the unsteady flow at 85% height. Hah et al focused on the unsteady aerodynamics using a 3D, non-linear, unsteady CFD model. Both papers show some encouraging agreement between computation and experiment, but also indicate that there may be some difficulties with the modelling, and that further consideration of the level of modelling required for forced response prediction would be useful. For example, while Hah et al show complex 3D phenomena in the unsteady flow, Manwaring et al's unsteady model is based on the premise that an essentially 2D model will capture major effects.

Further evaluations of computational models against the ADLARF test data are presented in this paper and the companion paper by Bréard et al (2000). Bréard et al present results from a coupled structural-fluid, 3D, non-linear, unsteady model. Here, further computational results from a 3D, linearised, unsteady Euler method and a different 3D, non-linear unsteady model are reported. Results from the various models are compared and discussed. The aim is to demonstrate what can be achieved with present models, and to indicate areas where further work is needed.

THE STRUCTURAL MODEL

Structural modelling was undertaken in a proprietary automatic analysis system, early developments of which are described by Armstrong and Edmunds (1989). A finite element model of the blisk structure was constructed using the measured blade co-ordinates. An approximate representation of the disc was included in the model, and gas pressure loads were interpolated from a CFD solution. This model was used to calculate the running blade shape and the vibration modes. These were found to be in reasonable agreement with calculations and frequency measurements reported by Manwaring et al (1996). Fig. 2 shows a Campbell diagram summarising the vibration frequency results.

Fig. 2 shows frequency crossings for 1F/3EO, 2F/8EO, 1T/8EO and 2S/8EO modes, as is consistent with Manwaring et al's results. Agreement with the bench measurements is good, although the 2F mode frequency is

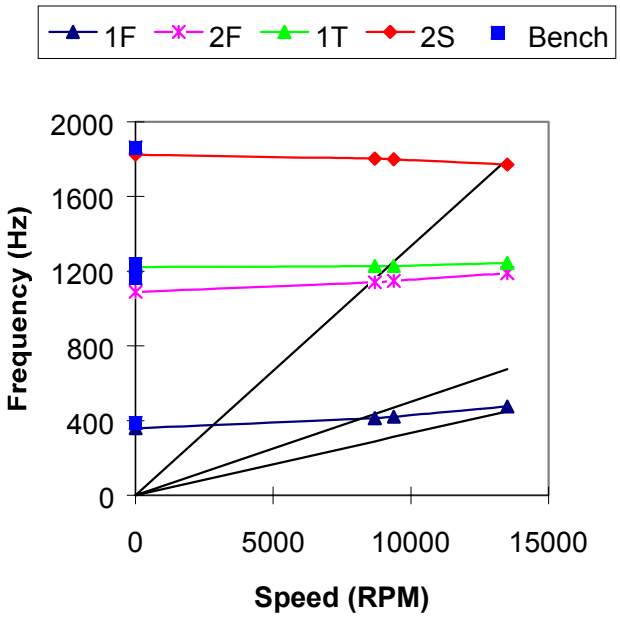

Fig. 2. Campbell Diagram

slightly underpredicted. However, the 2F/8EO and 1T/8EO crossings are coincident in Manwaring et al's model, whereas they are distinct in the present calculations. This is possibly due

to underprediction of the 2F mode frequency. It may also be noted that Manwaring et al anticipated a 1F/2EO crossing at 105% speed, but this was not obtainable during testing.

As will be explained below, this structural model was used in obtaining predictions for the three resonant conditions studied experimentally. These are summarised in table 1.

Mode	% Mechanical speed N1	% Aerodynamic speed N1/√T
1F	62	66
2F/1T	68	69
2S	98	100

Table 1. Summary of resonant conditions considered.

THE AERODYNAMIC MODELS

The 3D, linearised, unsteady, inviscid solver used here is based on that described by Giles (1992) and Marshall and Giles (1997). This method works in the frequency domain, and takes advantage of the assumed periodicity and small amplitude of the unsteadiness to give efficient computation of the unsteady flow. Blade movement can be included in the model, using a mesh movement algorithm and a modal representation of the structural model. Structured, 'H-type' meshes are employed with a mesh size of 31(circumferential) x 121(axial) x 25(radial) for the present calculations. The inlet and exit boundary conditions are as formulated by Giles (1990) to avoid pressure wave reflections in 2D flows. All calculations have been done on a single blade passage with the appropriate 'inter-blade phase angle' being specified to give the correct periodicity for the unsteady calculations. Tip clearance effects are not included in this model.

The 3D, viscous, non-linear, steady and unsteady solvers used by the present authors are developments of the methods described by Denton (1992). These programs use 'H-type', structured meshes and for all the results presented here a mesh size of 41(circumferential) x 205(axial) x 49(radial) per blade passage has been used. There were 84 axial mesh locations within the blade passage. A simple 'pinched tip' was used to model the rotor tip gap, with a single radial cell of 0.33% blade span between the blade tip and the casing. A simple mixing length turbulence model is used in these models. Exit boundary conditions used for this case were similar to those for the linear model. Inlet conditions for the unsteady calculations involved specification of stagnation pressure, stagnation temperature and flow angle distributions, and did not include any special treatment to avoid reflections. However, for the conditions considered, upstream propagating waves are sufficiently weak for the effect of reflections to be negligible. This was confirmed by numerical experiments for 'clean' inlet conditions. While steady calculations were done using a single blade passage, the domain was extended to 2 blade passages for the 8 engine order (8EO) inlet distortion, as this allowed periodicity to be assumed. With this assumption any non-linear waves travelling in the circumferential direction are neglected.

Bréard et al's (2000) CFD model is based on that described by Vahdati and Imregun (1995). The program allows use of unstructured meshes, and solves the 3D viscous, non-linear, steady and unsteady equations with a Baldwin-Barth turbulence model. As for the linearised solver, blade movement can be included using a modal structural model. For the ADLARF computations, Bréard et al used mixed element, semi-structured meshes with about 180 000 mesh points per blade passage. The formulation of the inlet and exit boundary conditions is such as to avoid reflections in the idealised case of one-dimensional flow. For the unsteady calculations, the domain included 2 passages for the 8EO inlet distortion and the full annulus (16 blades) for the 3EO distortion.

STEADY AERODYNAMICS

With only limited data available regarding the aerodynamic performance of this fan, some assumptions had to be made regarding the inlet and exit boundary conditions. Total pressure and temperature, and flow angle are specified at the inlet. These were estimated from the circumferential averages of the measured values with the inlet distortion screens fitted for the 8 distortion/rev, 68% speed case. For initial calculations, radial distributions of the circumferentially averaged static pressure were specified. These were estimated from a throughflow calculation for the rotor using the available pressure data. As indicated below, further calculations were performed with pressure specified just at one point on the casing at exit. The latter method for specifying the exit boundary condition was also adopted by Hah et al (1996).

A comparison of various calculations of the blade pressure distribution at 88% span for the 98% shaft speed condition is shown in fig 3a. Other workers' comparisons of CFD results for compressor performance (e.g. Dunham, 1998) have shown considerable differences between different codes and models. Hence the difference between the present results and those of Bréard et al (2000) is not surprising. The surface pressure plots and Mach number contours in fig. 3 reveal a complex shock structure within the passage. Overall mass flows and pressure ratios from the two viscous models are in reasonable agreement. Comparison of the present Mach number plots with those of Bréard et al shows different suction surface boundary layer thickness downstream of the shock, the present model giving a thinner boundary layer. The surface pressure distributions are similar to those of Manwaring et al (1996). Manwaring et al's results indicate a suction surface pressure minimum at about 60% chord, and a pressure surface maximum at about 50% chord.

Fig. 3a includes results from an inviscid, 3D model. These were obtained using the linearised unsteady Euler

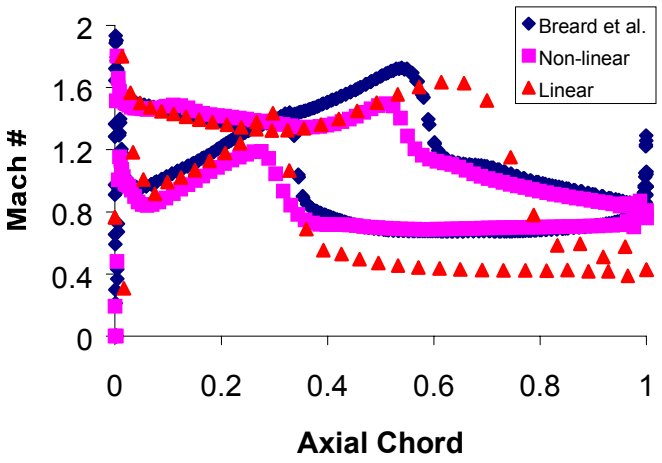

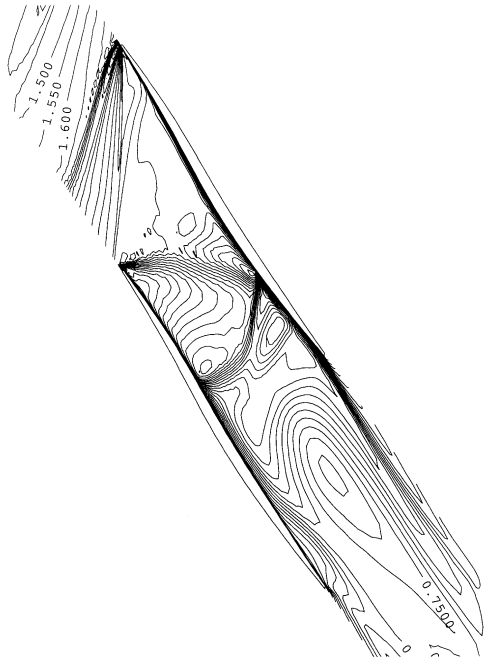

Fig.3. Mach number at 88% span for the 98% speed condition
(a) surface distributions
(b) contours (present non-linear model).

equation solver in steady mode. It had originally been intended to use 3D, viscous steady flow solutions as the basis for the linearised, unsteady analysis. This method has been used with some success by Chew et al (1998) for flutter analysis. However, for this case with strong tip leakage flows severe convergence difficulties were encountered in the attempted solution of the unsteady, inviscid equations, and the approach was abandoned. Instead inviscid steady solutions were used as the basis for the linearised unsteady analysis. Owing to lack of boundary layer blockage, the inviscid model can give quite different solutions to the viscous calculations. The practice adopted here was to tune the inviscid solutions to give reasonable shock positions by raising the exit pressure. This may be compared to Manwaring et al's procedure, which involved adjustment of the stream tube height in their quasi-3D inviscid code. The present 3D model does not give the option of stream tube adjustment. The difference between the suction surface shock position from the inviscid model and the two viscous models in fig. 3 reflects uncertainty in the viscous steady flow prediction, as the inviscid solution was tuned using a third viscous model that predicted a the shock position to be further downstream than in the other two models. Although these difficulties with the steady state modelling do present difficulties in interpreting the unsteady results, the present procedure does at least allow a qualitative comparison between linear and non-linear unsteady analyses.

A constant speed characteristic line was generated with the 3D viscous model by gradually increasing the back pressure to simulate the throttle process. This is shown in fig. 4. Apart from the datum point, the exit boundary conditions for these calculations involved specified static pressure at a single point on the casing. The predicted choking mass flow (corrected to standard sea level condition) is 74.3 kg/s, which is 2.3 kg/s higher than the design values quoted by Hah et al (1996) and Rabe et al (1995) for undistorted inlet conditions. However, Rabe et al give a value of 73.45 kg/s for the distorted inlet condition, which is considerably closer to the present calculations. Clearly the radial total pressure distribution at inlet affects the mass flow and uncertainties in this might well account for the discrepancy with Rabe et al's result. While this (and other) uncertainties should be noted, it is considered that the CFD solutions give a fair representation of the steady flow field.

Fig. 5 gives surface pressure profiles at 88% span for a 68% shaft speed condition. Here just Bréard et al's viscous solution and the inviscid solution are shown. Agreement between the two solutions is considerably better than for the high speed case. Bréard et al have done further calculations

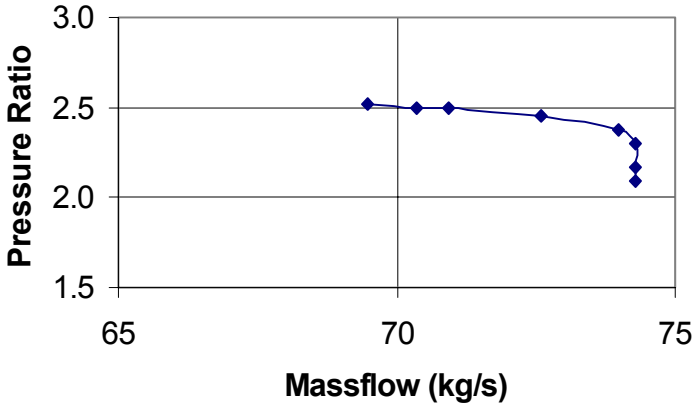

Fig. 4. Calculated operating map at 98% speed (present non-linear model).

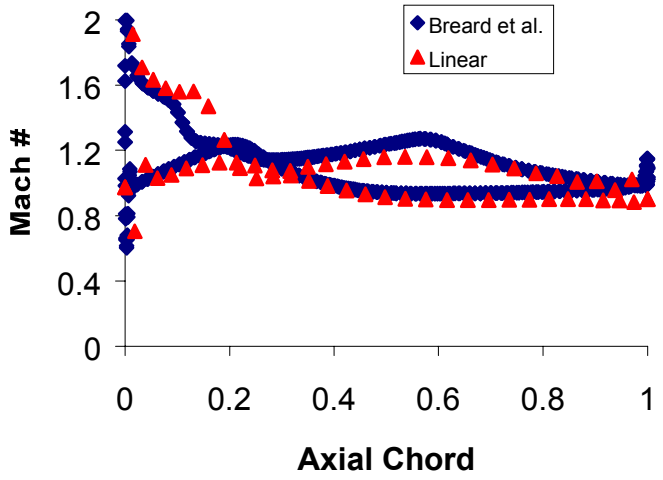

Fig. 5. Surface Mach number distribution at 88% span for the 68% speed condition.

varying the back pressure. Reasonable agreement with Manwaring et al's 3D viscous results has been found. Steady solutions for the 66% shaft speed condition were found to be qualitatively very similar to the 68% shaft speed case.

UNSTEADY AERODYNAMICS

Inlet boundary conditions for unsteady calculations were derived from the measured inlet distortion data. The data were Fourier analysed and the first harmonics were interpolated radially to obtain the 3D boundary conditions. For the non-linear calculations, inlet total pressure, total temperature and flow angle are specified. For the linear solver, the inlet boundary conditions are specified in terms of vortical, entropic and acoustic characteristics. As explained by Manwaring et al (1996), the inlet distortion in these cases is dominated by the vortical component with a further significant effect from the entropic component, and the resulting fluctuations in rotor incidence angle are up to ±4°.

8EO/2S Crossing at 98% Speed

The 8 distortion/rev, 98% shaft speed condition will be discussed in some detail in this section. Since the fan has 16 blades, non-linear calculations were performed on a domain extending over 2 passages with circumferential periodicity assumed. In order to achieve a periodic solution it was found necessary to extend the time marching procedure over about 20 periods. For the linearised, unsteady solution (in the frequency domain) the calculation extended over just one blade passage with the time lag between the solutions on the two circumferential boundaries expressed through an inter-blade phase angle. The time marching algorithm used to solve the linearised equations converges at a rate comparable to that for the solution of the steady flow.

Fig. 6 shows a comparison of predictions with differential pressure measurements at 88% span. These were

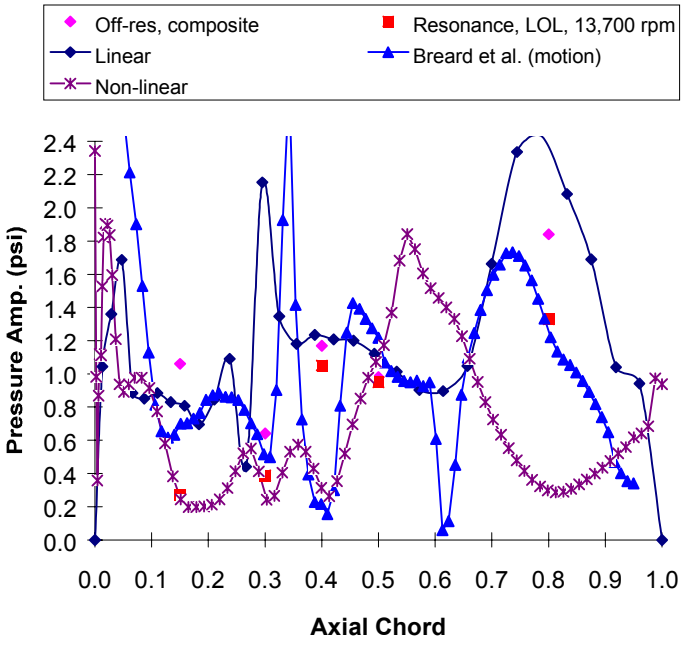

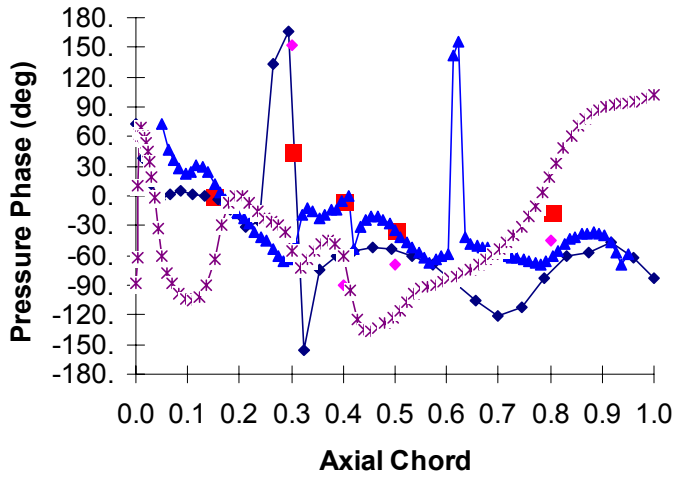

(b) phase

Fig. 6. Unsteady differential pressures at 88% span for the 98% speed condition.

obtained from transducers measuring the difference in pressure between suction and pressure surfaces of the blade. According to Woehr and Manwaring (1994) pressure transducers were fitted to 2 adjacent blades at 87.5% span. However, Manwaring et al and Hah et al (1996) report the instrumentation plane to be at 85% span. Hence there is a possibility of small differences between measurements and calculations due to this interpretation. Both measurements and calculations have been processed to obtain the first Fourier harmonic, and the amplitude and phase are shown in figs 6a and 6b, respectively. Phase data has been referenced to the first transducer, with the

relationship between the time scales for transducer signals and the rotor position being unknown. In the lack of further information relating the transducer and simulation time scales, any shift of phase between the calculated and measured results is allowable in comparing results. Two sets of experimental results are shown in the figure, off resonance and at resonance. The off resonance results were obtained by averaging measurements at conditions close to those of the calculation. Differences with the experimental results at resonant conditions are expected due to the blade motion, and might also be due in part to the change in the time-averaged operating point. Here attention should centre first on the off resonance conditions, as the present calculations do not include blade motion. Bréard et al's (2000) calculations included in fig. 6 do include a low level of blade motion, but this is reported to have had little effect on the differential pressures.

Comparing the various sets of results in fig. 6, it may first be observed that there is some fair agreement between experiment and calculation. However, there are also interesting differences between the different sets of results. Bréard et al's calculations are arguably closest to the measurements, but it is difficult to draw firm conclusions from this limited comparison. Bréard et al's results show a peak in the pressure differential at about 35% chord, the location of the shock on the pressure surface, and a dip around 62% chord which is just downstream of the shock on the suction surface in the steady solution. Considering the different modelling assumptions and steady solutions between the linearised, inviscid solution and Bréard et al's model, the differences between these two calculations are not surprising. In fact the results are sufficiently close to give encouragement for use of the much more computationally efficient linear methods. Differences between Bréard et al's results and the present non-linear calculations are perhaps more surprising and raise further questions. Effects of the pressure surface shock are not so pronounced in the present results, and the more forward position of the steady flow suction surface shock is clearly reflected in the unsteady results. The main difference in modelling assumptions between the present and Bréard et al's models are the turbulence models and the tip clearance. The present model has a tip gap clearance of 0.33 span, while Bréard et al did not include a tip gap in their unsteady model. Mesh dependency is also likely to contribute to differences in the results and numerical effects such as boundary condition treatment might also be significant.

The level of agreement between calculation and measurement shown in fig. 6 is similar to that shown by Hah et al, who give a comparison at the 80% chord position only. Manwaring et al's results from their quasi 3D, linear unsteady model (which includes blade motion) also show comparable levels of agreement with differential pressure measurements, although their phase predictions appear to show greater differences with measurements. Some uncertainty in the level of blade motion for this case should be noted. The trailing edge strain gauges installed for measurement of the 2S mode failed.

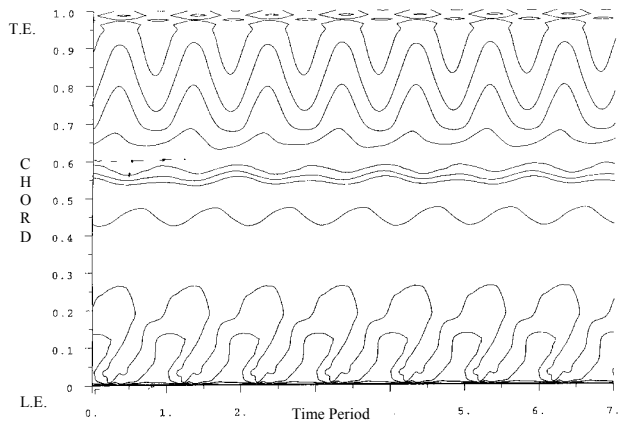

(a) suction surface.

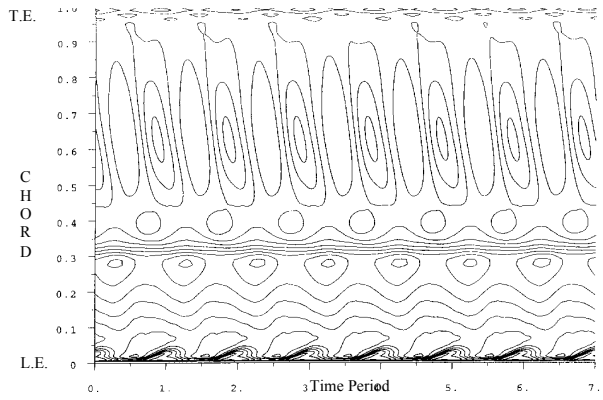

(b) pressure surface.

Fig. 7. Unsteady pressure contours at 88% span for the 98% speed condition.

Only blade root gauges were available to estimate vibration amplitudes, and these were described by Manwaring et al as 'marginally acceptable' for this purpose.

Further insight into the unsteady flow is given by the pressure contours in a time-chord plane shown in fig. 7. These were obtained from the present non-linear model. The periodicity in this figure confirms that the solution has converged. As might be expected, large amplitude fluctuations appear near the leading edge. More surprisingly, the highest pressure fluctuations appear at the rear of the blade, downstream of the shock. The shock itself only moves about 2 or 3% of chord. At 65% chord on the pressure surface the pressure fluctuation is about 1.7 times the maximum distortion in stagnation pressure at inlet.

Estimates can be made of the disturbance propagation speeds from the slope of the skewed contours in fig. 7. On the suction surface, upstream of the shock, an estimate of about 275 m/s is obtained. This is slower than the convection speed at a Mach number of about 1.55, but faster than the wave speed (fluid speed – speed of sound) of around 200m/s. The pressure pattern nevertheless shows that the pressure disturbances are

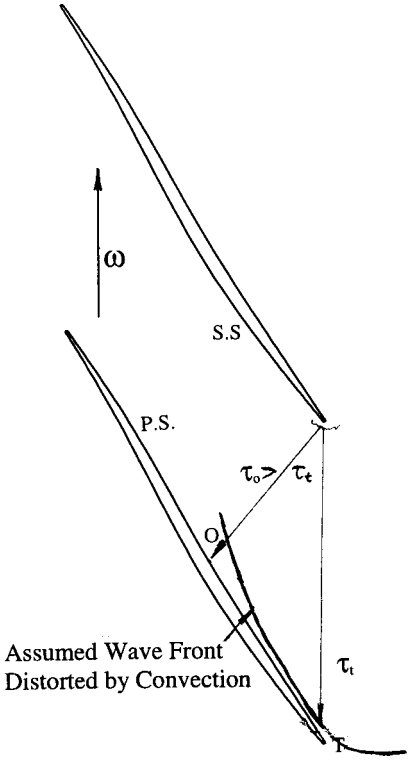

Fig. 8. Sketch of unsteady flow phenomena.

moving downstream from the leading edge. By contrast, downstream of the shock wave the pressure variation is not seen to be convective. Here the disturbances are almost like standing waves and vary in phase along the rear 40% of chord. The exact source of such pressure variations is not clear, but one likely source is strong trailing edge vortex shedding or flow flapping due to the high loading variation caused by the inlet distortion. This fluctuation may also excite the shock motion, which could in turn enhance the loading variation and hence the vortex shedding.

On the pressure surface, the shock movement is out of phase with that on the suction surface. This indicates that the shocks in adjacent blade passages are out of phase. It is interesting to note that, on this surface, the pressure disturbances seem to travel upstream at much higher speeds. Upstream of the shock the speed is estimated to be about 330 m/s. Downstream of the shock the contour pattern is steeper and the speed is estimated at about 550 m/s. It is likely that waves from the adjacent blade trailing edge arrive at the surface with quite large inclination angle, resulting in high upstream propagating phase velocity on the pressure surface. This is illustrated in fig. 8. The sketch shows a wave front from the trailing edge of one blade arriving at the pressure surface of the next wave. The wave front propagation is distorted by the mean velocity field and it arrives first at the trailing edge. The propagating velocity on this part of the pressure surface could be estimated as $OT/(\tau_t-\tau_o)$. Upstream of the shock, although the local speed is supersonic, the component along the wave direction is still subsonic and the upstream propagating waves appear to have slightly lower phase velocity. It is also interesting to note that the blade spacing at this height is about half the acoustic wavelength of the unsteadiness. High pressure fluctuations at this blade height could be the result of resonance between the shock motion and the trailing edge flow flapping.

8EO/2F/1T Crossing at 68% Speed

Comparisons of the present linear model results with those of Bréard et al and the measured data are given in fig. 9. The present non-linear viscous model was not applied to this case. The results from Bréard et al presented here do not

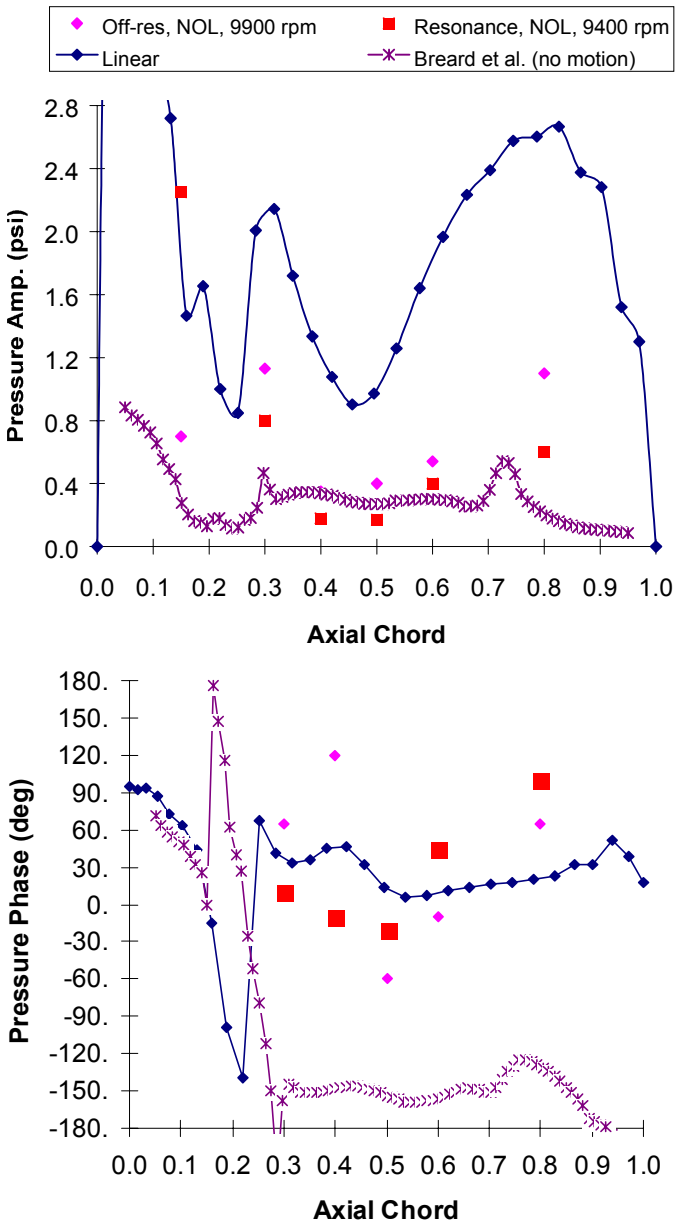

Fig. 9. Unsteady differential pressure at 88% span for the 68% speed condition.

include blade motion and so differ somewhat from those given in the companion paper. It may be noted that the blade motion at resonance will be an unknown combination of the 2F and 1T modes. Further complications may arise from blade-to-blade differences or mistuning. As discussed by Manwaring et al, strain gauge measurements on adjacent blades indicate a phase difference of 121.5° compared to the assumed (fully tuned) value of 180°.

Note, in fig. 9b, that Bréard et al's results show a very rapid change of phase on the 15% chord location where the phase is datumed. Adjustment of the datum position would give much better apparent agreement with the experimental data. Thus the general level of agreement between Bréard et al's results and the data is reasonable, although the calculated amplitude is rather low towards the rear of the blade. The linear model seems to overpredict the amplitude of the pressure perturbation. For this case the calculations of Manwaring et al and Hah et al appear to be in closer agreement with data towards the rear of the blade than are the results in fig. 9. This may be associated with differences in the steady surface pressure distribution to that reported by Manwaring et al for their resonant condition. A further observation is that a significant part of the difference between the off resonance and at resonance measurements is probably due to the different (steady) operating point, rather than just blade motion. Bréard et al have demonstrated some sensitivity to the steady flow conditions and, extrapolating their results to the more rearward suction surface shock shown by Manwaring et al gives a significantly higher pressure in this region. It may be that uncertainties in the steady operating condition have contributed to the differences in the unsteady solution from the measurements.

There is no obvious explanation for the overprediction of amplitude by the linear model. Although the lack of viscous dissipation of the distortion in the inlet might be expected to lead to some overestimate of the forcing, this was not apparent for the 98% speed condition. Manwaring et al's results, which are also from a linear model, give better agreement with measurement. This could indicate that the discrepancy might be associated with the use of a modified exit pressure to 'tune' the inviscid steady solution, rather than a basic limitation of the linear, inviscid unsteady flow assumptions. In their quasi-3D model Manwaring et al adjusted the stream tube height distribution to match with a 3D steady flow CFD solution.

3EO/1F Crossing at 62% Speed

For this condition comparison of calculated and measured pressure differentials are shown in fig. 10. Again the present non-linear model was not applied to this case. For this 3 periods/rev distortion Bréard et al's calculation included the whole annulus. As for the 68% speed case above, Bréard et al have looked at the sensitivity to exit flow boundary conditions. The results here are for the original estimate of the boundary conditions, without blade motion and differ slightly from those in the companion paper

Bearing in mind that a shift in phase is allowed, Bréard et al's results agree very well with the data in fig. 10. The linear model also predicts the phase well but, as in section 5.2, overpredicts the amplitude significantly. Again this is not understood at present and requires further study. Manwaring et al were unable to obtain predictions at this condition and Hah et al did not consider this case.

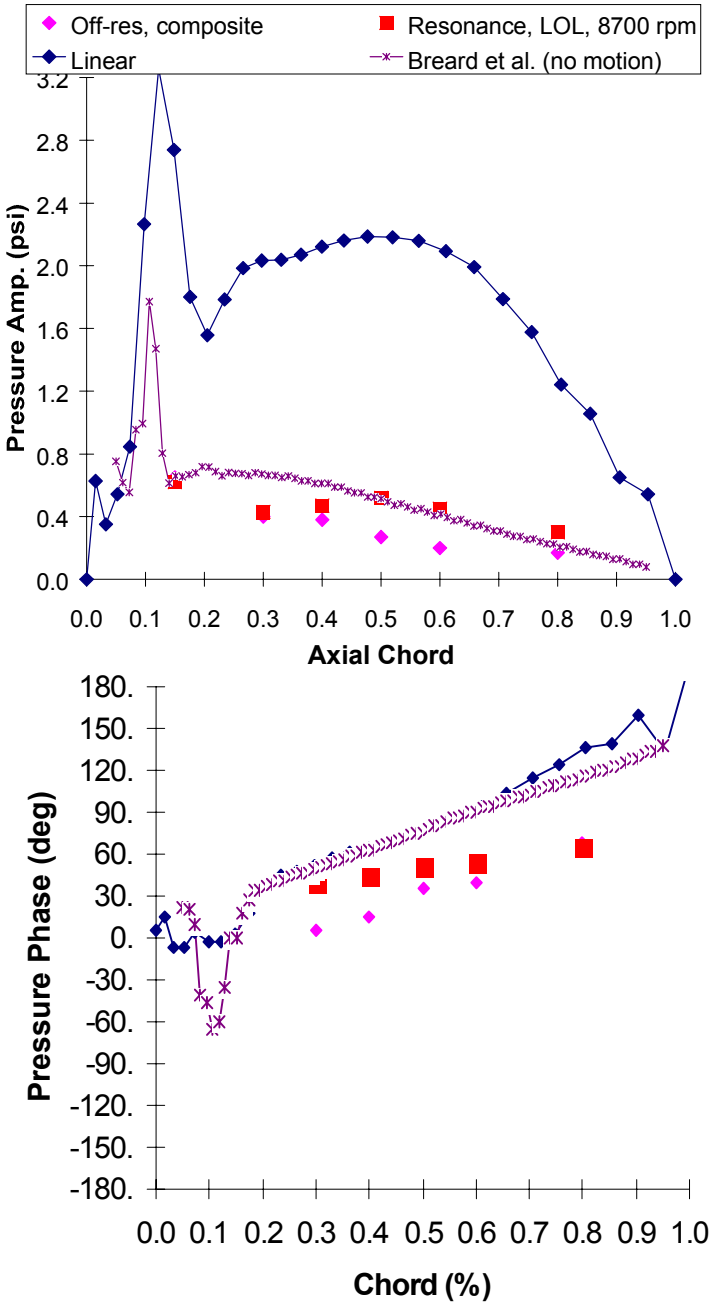

Fig. 10. Unsteady differential pressure at 88% span for the 62% speed condition.

STRUCTURAL RESPONSE

The present linear model has been used to estimate the aerodynamic damping of the blade vibration. To do this the vibration modeshape is first interpolated onto the blade surface mesh in the aerodynamic model. The unsteady flow due to blade vibration is then computed and the resulting unsteady modal force distribution on the blade calculated. Integration of force times velocity over a vibration period and the blade surface then gives the net energy transfer between the blade and the air. This will, of course, depend on vibration amplitude. With the linear (or small perturbation) assumption, superposition may be used to calculate the combined effect of the inlet distortion and blade motion. The modal equation of motion for the blade can then be used to calculate the vibration amplitude due to the inlet distortion.

Results from the aerodynamic damping calculations are summarised in table 2. These are presented in the form of a Q factor. From linear theory with an assumed form of the damping, this corresponds to $\omega_m/\Delta\omega$, where $\Delta\omega$ is the width (difference of frequencies) on a frequency against response amplitude plot at which the amplitude equals $1/\sqrt{2}$ times the peak value ω_m. Low values of Q correspond to high damping and vice versa. Bréard et al (2000) estimated values from the results of their coupled non-linear model assuming linear behaviour in extracting the influence of blade motion alone. Manwaring et al (1996) gave estimates from the strain gauge results on two adjacent blades. Comparing the three sets of results indicates better agreement between Bréard et al's viscous non-linear model and measurement than is obtained with the linearised, inviscid model. For the 8EO/2F/1T crossing, where the agreement is not very good, it should be noted that Bréard et al assumed exact coincidence of the two modes and estimated damping for each mode. From the test Manwaring et al identified a two peak response, possibly associated with the two modes. Formation of combined modes is also likely. For all cases the scatter between different blades and the difficulties involved of deducing an accurate estimate of damping from the data should be noted.

Stress levels at the strain gauge position may be estimated from the structural model using the vibration amplitudes given by the linear model. Bréard et al have applied a similar procedure to estimate limiting vibration displacements (since it is computationally very expensive to run the non-linear model to find the vibration amplitude) and these may also be converted to stress levels. Comparison of the two sets of calculations shows significant differences. However, with uncertainties regarding the exact blade geometry at the hub and the strain gauge positions and orientation a worthwhile comparison has not been possible in the present study.

CONCLUSIONS

State-of-the-art methods have been applied to study forced response due to inlet distortion and results have been compared to other workers' measurements from an advanced transonic fan tested in the Compressor Research Facility at Wright-Patterson Air Force Base. Three resonance crossing points were considered, with greater attention focused on the 8EO/2S crossing at 98% shaft speed. While some uncertainties regarding both the modelling assumptions and experimental data have been noted, some conclusions can be drawn from this work and are summarised below. Overall, the level of agreement between calculations and measurements is considered encouraging for application of CFD-based methods for forced response prediction, although there are certainly areas where further research is needed. The present results and conclusions build on and extend earlier model evaluations by Manwaring et al (1996) and Hah et al (1996) and the companion paper by Bréard et al (2000).

% Speed N1/√T	crossing	Aero damping (Q factor)		Total damping (Q factor)
		linear model	Bréard et al	Manwaring et al Blade 1(Blade 16)
66	3EO/1F	93	60	63 (50)
69	8EO/2F 8EO/1T	639 461	45 80	156 (238)
100	8EO/2S	125	100	82 (71)

Table 2 Summary of aerodynamic damping and blade response results.

Mixed results were obtained from a 3D, inviscid, linearised unsteady CFD model. Although results for the 8EO/2S crossing at 98% speed were encouraging, overprediction of the blade pressure perturbation amplitude was found at the other two crossings. To some extent these discrepancies conflict with Manwaring et al's results from a 2D, inviscid, linearised model, and are not fully understood. This apparent discrepancy may be due to the need to artificially reduce the exit pressure to obtain a reasonable inviscid steady flow solution. Attempts to use a viscous steady solution as the basis for the linearised solution failed in this case due to the strong over-tip leakage flow. An improvement on the present model might be obtained by using a viscous steady solution that neglects tip clearance effects. However, 3D viscous linearised methods are now becoming available and, with inclusion of viscous effects it should be possible to obtain unsteady solutions that include the tip clearance. Linearised methods have a clear advantage over non-linear methods in terms of computational efficiency.

Bréard et al's 3D, viscous, non-linear model generally shows a reasonable level of agreement with measurements for both blade pressures and blade response. It is certainly encouraging that the less restrictive assumptions in this model have lead to better agreement with data. The present study is one in a series of evaluations that are building confidence in this model for application to aeroelasticity problems in turbomachinery. However, some areas of uncertainty should be

noted. Difficulties with the prediction of steady flow in transonic fans have been encountered by other workers and are reflected in differences between steady solutions from the two 3D, viscous codes presented here. Manwaring et al's measurements clearly show blade-to-blade differences that are not captured in the 'fully-tuned assembly' model. The effect of a frequency separation of the two modes for the 8EO/2F/1T crossing has not been investigated. Also, the full non-linear treatment in the model is compromised to some extent by resorting to the assumption of some linear behaviour in deriving the limiting blade amplitude. These assumptions can be addressed but application is currently limited by computational expense of the method.

For the 98% speed case the flow has been considered in some detail. Steady calculations show the rotor to have a complex shock wave system and a very strong over tip leakage effect through a relatively small tip gap. The unsteady calculations reveal a large pressure fluctuation downstream of the main passage shock towards the rear of the passage, especially on the pressure surface. The surface pressure fluctuation peaks at 170% of inflow unsteadiness in stagnation pressure. The most likely origin of this unsteadiness is considered to be the trailing edge. Trailing edge vortex shedding or flow flapping may be excited by the high loading variation due to the inlet distortion. This interpretation of the unsteady flow differs from that of Hah et al who attribute increased loss in the outer part of the blade to strong shock-boundary layer interaction, resulting in a vortex being convected downstream.

Given the known sensitivity of transonic fan CFD results to modelling assumptions it is not surprising that there is evidence of such sensitivity in the unsteady calculations. For the 98% speed condition, the present viscous model indicated shock movements of around 2% of chord, compared to shock movements of up to 20% of chord movements reported by Hah et al from their calculations. These differences in results are likely to be associated with different treatments of the boundary layer and, in particular the state of the layer downstream of the shock could be important. It is certainly questionable whether current models will capture the shock-boundary layer interaction correctly. Further computations with the present model have been performed by rotating the inlet distortion very slowly relative to the blade. In this case, for which the flow is expected to be 'quasi-steady', the shock was found to move on the surface over about 20% of chord. Thus the discrepancy with Hah et al's results appears to be associated with inertial effects.

ACKNOWLEDGMENTS

Assistance from a number of our colleagues at Rolls-Royce and Imperial College is gratefully acknowledged. Particular thanks are given to M. Hall, S. Lee and N. Smith for their roles in setting up the project, constructing the basic structural model and conducting the throughflow analysis.

Funding from the Ministry of Defence and provision of data by the US Air Force is also gratefully acknowledged.

REFERENCES

Armstrong, I.A. and Edmunds, T.M., 1989. Fully automatic analysis in the industrial environment. Proc. Second Int. Conf. on Quality Assurance and Standards in Finite Element Analysis, NAFEMS.

Bréard, C., Vahdati, M., Sayma, A.I. and Imregun, M., 2000. An integrated time-domain aeroelasticity model for the prediction of fan forced response due to inlet distortion. Paper proposed for ASME Gas Turbine Expo.

Chew, J.W., Hamby, R.J., Marshall, J.G. and Vahdati, M., 1998. Part speed flutter of transonic fans. Proc. PEP Symp. On Design Principles and Methods for Aircraft Gas Turbine Engines, Paper 26, Toulouse, France.

Denton, J.D., 1992. The calculation of 3 dimensional viscous flow through multistage turbomachines. ASME J. Turbomachinery, 114, No 1.

Dunham, J. (ed.), 1998. CFD validation for propulsion system components. AGARD advisory report AR355.

Giles, M.B., 1992. An approach for multi-stage calculations incorporating unsteadiness. ASME paper 92-GT-282.

Hah, C., Rabe, D.C., Sullivan, T.J. and Wadia, A.R., 1996. Effects of inlet distortion on the flow field in a transonic rotor. ASME paper 96-GT-547.

Manwaring, S.R., Rabe, D.C., Lorence, C.B. and Wadia, A.R. 1996. Inlet distortion generated forced response of a low aspect ratio transonic fan. ASME paper 96-GT-376.

Marshall, J.G. and Giles, M.B., 1997. Some applications of a time-linearized Euler method to flutter and forced response in turbomachinery. Proc. 8th Int. Symp. On Unsteady Aerodynamics and Aeroelasticity of Turbomachines, Stockholm, Sweden.

Rabe, D.C., Bolcs, A. and Russler, P. 1995. Influence of inlet distortion on transonic compressor blade loading. AIAA paper 95-2461, 31st Joint Propulsion Conference, San Diego, USA.

Vahdati, M. and Imregun, M. 1995. Non-linear aeroelasticity analyses using unstructured dynamic meshes. Proc. 7th Int. Symp. On Unsteady Aerodynamics and Aeroelasticity of Turbomachines, Elsevier Pub.

Woehr, D.A. and Manwaring, S.R., 1994. Augmented damping of low aspect ratio fans (ADLARF). USAF report, WL-TR-95-2008.

